Applied Surface Science 507 (2020) 145095

Contents lists available at ScienceDirect

Applied Surface Science

journal homepage: www.elsevier.com/locate/apsusc

Full Length Article

Incorporating highly dispersed and stable Cu^+ into TiO_2 lattice for enhanced photocatalytic CO_2 reduction with water

Zhuo Xiong[a], Zuwei Xu[a], Youzi Li[a], Liangchen Dong[a], Junyi Wang[a], Jiangting Zhao[a], Xiaoxiang Chen[b], Yongchun Zhao[a,*], Haibo Zhao[a,*], Junying Zhang[a]

[a] State Key Laboratory of Coal Combustion, School of Energy and Power Engineering, Huazhong University of Science & Technology, 1037 Luoyu Road, Wuhan 430074, China

[b] College of Environmental Engineering, Wuhan Textile University, 1 Sunshine Avenue, Wuhan 430200, China

ARTICLE INFO

Keywords:
CO_2 photocatalytic reduction
Cu^+ doping
TiO_2
Dispersion
Stability

ABSTRACT

Cu-based catalysts have been widely studied for photocatalytic CO_2 reduction; however, the role of Cu species is still ambiguous because they exist in multiple forms, which can possibly interchange between themselves. In this paper, highly dispersed Cu^+ was incorporated into a TiO_2 lattice through a flame spray pyrolysis (FSP) route, and it exhibited excellent activity and stability for photocatalytic CO_2 reduction. The highest CO and CH_4 yields were obtained on CuTi-1, reaching 43.5 and 16.7 μmol g^{-1} after 4 h of irradiation, which are 2.8 times and 8.4 times higher than those of pristine TiO_2, respectively. After three cycles, the activity of CuTi-1 only slightly decreased. The highly dispersed Cu^+ ions in the TiO_2 lattice were very stable, and they effectively slowed the recombination of the photoinduced charges, which was confirmed by XPS and PL analyses. Meanwhile, the Cu^+ ions in the TiO_2 lattice promoted the adsorption and activation of CO_2 and served as the active sites for CO_2 photoreduction.

1. Introduction

Photocatalytic CO_2 reduction with water is regarded as a good solution to global warming [1–4]. Since the pioneering work finished by Inoue et al. [5] in 1979, TiO_2 has become a very popular photocatalyst due to its practicality, stability, good economy, and low toxicity [6,7]. However, the photocatalytic activity of TiO_2 for CO_2 reduction is too low due to the fast recombination of photoinduced charges and limited utilization of visible light [8].

Modifying TiO_2 with a metal such as Cu [9–11], Pt [12–14], or Ag [15–17] has been reported as an effective route to enhance CO_2 photocatalytic reduction because the metal can improve the charge separation, light absorption, or CO_2/H_2O chemisorption, etc. Among them, Cu-modified TiO_2 has attracted wide attention [18–20] due to the good performance and low cost of Cu. It has been reported that the Cu species in the Cu/TiO_2 catalyst could have multiple chemical states (Cu^0, Cu^+, and Cu^{2+}) and exist in many forms (e.g., ions doped into a TiO_2 lattice or oxide deposited on a TiO_2 surface) [19,21,22]. This provides a possible route to tune the properties of Cu/TiO_2 catalyst, but on the other hand, this also makes it difficult to clearly understand the roles of Cu species because of the co-existence of Cu species with different oxidation states and/or the existence or various forms in Cu/TiO_2 catalysts and the possible interchange between them during the CO_2 photoreduction reaction [23,24]. For example, Tseng et al. [18] reported the coexistence of Cu^+ and Cu^{2+} in a sol-gel derived Cu/TiO_2 catalyst, and Cu^+ was found to be the active site for photocatalytic CO_2 reduction. Later, Li et al. [24] found that Cu^+, the active sites in mesoporous Si-supported Cu/TiO_2 catalysts, were reduced to Cu^0 by photoinduced electrons during the CO_2 photoreduction reaction, which may be responsible for the deactivation of Cu/TiO_2. Our group [23] also observed the reduction of Cu^+ to Cu^0 during CO_2 photoreduction over Cu_2O deposited TiO_2 nanocrystals, decreasing the photocatalytic activity. However, Tan et al. [25] reported that the deposition of Cu^0 nanoparticles on the TiO_2 surface greatly enhanced CO_2 photoreduction due to the localized surface plasmon resonance (LSPR) of Cu^0 nanoparticles. In addition, Liu et al. [20] and Chen et al. [22] demonstrated the coexistence of Cu^+ and Cu^0 in H_2-pretreated Cu/TiO_2 and suggested that Cu^0 could be oxidized into Cu^+ by photogenerated holes. More recently, Yuan et al. [26] observed that, during CO_2 photoreduction, the Cu(II) dispersed on mesoporous TiO_2 was reduced to Cu(I) and finally Cu(0) and found that the mixed Cu(I) and Cu(0) were more effective for the evolution of CH_4. As seen, the roles of Cu species are very complex and deserve in-depth exploration and identification.

To better understand the roles of Cu species in CO_2 photocatalytic

* Corresponding authors.
E-mail addresses: yczhao@hust.edu.cn (Y. Zhao), hzhao@hust.edu.cn (H. Zhao).

https://doi.org/10.1016/j.apsusc.2019.145095
Received 26 September 2019; Received in revised form 4 December 2019; Accepted 16 December 2019
Available online 23 December 2019
0169-4332/

reduction, it is important to synthesize a stable Cu/TiO_2 model catalyst with a sole Cu oxidation state and form. In our previous work [27–29], Cu-modified TiO_2 catalysts were prepared by the flame spray pyrolysis (FSP) method, and we found that the doping content of Cu greatly affects its oxidation states and forms of existence. Cu^+ ions were the primary Cu species and were doped into the TiO_2 lattice in a low Cu content. While at a higher Cu content, more CuO and Cu_2O nanoclusters or even nanocrystals formed on the TiO_2 surface. Therefore, it is possible to prepare a Cu^+/TiO_2 model catalyst by rationally controlling the synthetic conditions of the FSP process.

In this paper, TiO_2 nanoparticles with highly dispersed and stable Cu^+ doped into the lattice (CuTi) were synthesized by the FSP method and were used as a model catalyst to study the role of doped Cu^+ in the CO_2 photocatalytic reduction. The oxidation state, form of existence, and distribution of Cu species were confirmed. The effects of Cu^+ incorporation on the morphology, light absorption, and charge separation of CuTi catalysts were characterized. The photocatalytic CO_2 reduction performances of CuTi catalysts were studied, and the relationship between them and Cu^+ doping was established. The role of Cu^+ dopant in the activation and transformation of CO_2/H_2O was explored, and the active sites were identified.

2. Experimental

2.1. Synthesis of the photocatalyst

Highly dispersed Cu^+ was incorporated into the TiO_2 lattice by using the FSP system (NPS10, Tethis, Italy) reported in our previous works [29,30]. Typically, a certain amount of $Cu(NO_3)_2{\cdot}3H_2O$ was dissolved into a mixed solution of titanium butoxide (TBOT) and ethanol (17 vol% TBOT). Then, the mixed precursor solution was dispersed into fine droplets through a two-fluid atomizing nozzle and ignited by a pilot CH_4/O_2 annular flame. The solid combustion products were collected by a glass fibre filter and labelled as CuTi-0.5, CuTi-1, and CuTi-2 according to the designated molar ratios of Cu/(Cu + Ti) (0.5 mol%, 1 mol%, and 2 mol%, respectively). The flow rates of precursor solution and the dispersion gas (O_2) were 5 mL min^{-1} and 5 L min^{-1}, respectively.

2.2. Catalyst characterization

For all catalysts, the crystal lattice structure and parameters were tested by an Empyrean X-ray diffractometer using Cu Kα radiation (λ = 0.1542 nm). The surface area and porosity were analysed by a Micrometrics analyser (ASAP 2020) through N_2 adsorption–desorption. The chemical states of surface elements were determined on an X-ray photoelectron spectroscopy (XPS) instrument (Shimadzu/KRATOS AXIS-ULTRA DLD-600W). Transmission electron microscopy (TEM) images were acquired on an FEI Tecnai G^2 F30 instrument. The electron-hole recombination characteristics were obtained from photoluminescence (PL) spectra with excitation by a 325 nm laser using a LabRAM HR800c focal laser Raman microscope. The absorption of incident light was obtained from UV–vis diffuse reflectance spectra (DRS) collected by a UV–vis spectrophotometer (Perkin Elmer, Lambda950).

The in situ diffuse reflectance infrared Fourier transform spectra (DRIFTS) were collected on a Nicolet iS50 spectrometer (Thermofisher). The in situ experiments were conducted in a Harrick reaction chamber with two ZnSe windows and another quartz window, which are used for IR and UV light transmission, respectively. CO_2 and water co-adsorption in the dark were first investigated by passing CO_2 and a water vapour mixture into the reaction chamber at 30 °C for 15 min. Then, the Xe lamp was switched on to study the transformation of CO_2 species during the photocatalytic reaction.

2.3. Photocatalytic CO_2 reduction

Photocatalytic CO_2 reduction was performed at 120 °C in a successive-flow reactor reported in our previous work [13,31]. The light source (300–400 nm, 7.3 mW cm^{-2}) was supplied by a 300 W Xe arc lamp. Typically, a thin film of catalyst (10 mg) was deposited on a glass plate put in the photoreactor. Before illumination, the reactor was first purged with a mixture of CO_2 and water vapour (4.4 vol% water) for 1 h at 200 mL min^{-1} and then 0.5 h at 5 mL min^{-1}. Next, the Xe lamp was turned on and the photocatalytic experiment began. The concentrations of gaseous products were analysed every half an hour by a gas chromatography (GC) using a thermal conductivity detector (TCD) and a flame ionization detector (FID).

To verify that all carbonaceous products came from CO_2 reduction, a series of blank experiments was performed as follows: first, a mixture of CO_2 and H_2O vapour was used as the reactants in the empty reactor or reactor with only a Petri plate in it. The results showed that, in the above two cases, no carbon-containing products were generated in the dark or under light, proving that CO_2 photoreduction failed to happen without photocatalyst. Second, N_2 was used to replace CO_2 in a CO_2/water vapour mixture to perform the reaction in the presence of photocatalyst. No carbonaceous products were detected under light, demonstrating that all carbon-containing products originated from CO_2.

3. Results and discussion

3.1. Characterization

Fig. 1A shows that the TiO_2 in all samples has two phases: anatase and rutile. The intensity of the main rutile peak ($2\theta = 27.44^{\circ}$) increased gradually as the copper doping ratio increases, indicating the promotion of the transformation of anatase to rutile by Cu doping. With the increase of the copper doping ratio, the full width at half maximum (FWHM) of the main peak is nearly constant, indicating less variation in the particle size of the as-synthesized samples. No peaks corresponding to CuO or Cu_2O were detected in all CuTi samples, which means that no large CuO or Cu_2O crystals were formed in CuTi catalysts. This is because, in the FSP process, the composites can be mixed at an atomic level, which inhibits the formation of large Cu oxide crystals [32,33]. In our previous work [30], no Cu oxide crystals were detected in FSP-made Cu/TiO_2 particles even when the Cu content reached 20 wt%. Notably, as shown in Fig. 1B, the main peak of CuTi samples moved to a lower diffraction angle, indicating the expansion of the TiO_2 cell volume. Considering the larger radii of Cu^+ (96 pm) and Cu^{2+} (72 pm) than that of Ti^{4+} (68 pm), this result basically proved the possible substitution of Ti^{4+} in TiO_2 by Cu ions. [13,28,34].

Fig. 2 shows the TEM images of all samples with their particle distributions, indicating that TiO_2 particles are basically spherical nanoparticles with an average size of approximately 10 nm. The co-existence of anatase and rutile TiO_2 phases was observed based on the interplanar spacing in HR-TEM images, which is consistent with the XRD results. However, no Cu_2O or CuO crystals were clearly observed in the TEM and HR-TEM images of CuTi samples. In our previous work [30], we found that even when the Cu concentration reached 12%, it is still difficult to clearly observe the Cu oxide crystals in the TEM images of FSP-synthesized Cu/TiO_2. EELS mapping (Fig. 2E-H) shows the distributions of Cu, Ti, and O elements in the CuTi-1 sample. Fig. 4H shows that Cu was highly dispersed in the CuTi-1 sample. Therefore, combining the results of XRD, it can be known that the Cu species were highly dispersed and could exist as dopants incorporated into the TiO_2 lattice rather than as Cu_2O/CuO crystals deposited on the surface of TiO_2.

The XPS spectra in Fig. 3A show that the Cu $2p_{3/2}$ peaks for CuTi-0.5 and CuTi-1 were both located at approximately 932.5 eV, demonstrating that the Cu in CuTi-0.5 and CuTi-1 existed as Cu(I) [22,35]. Merely, the Cu $2p_{3/2}$ peak of CuTi-2 can be fitted into two peaks located

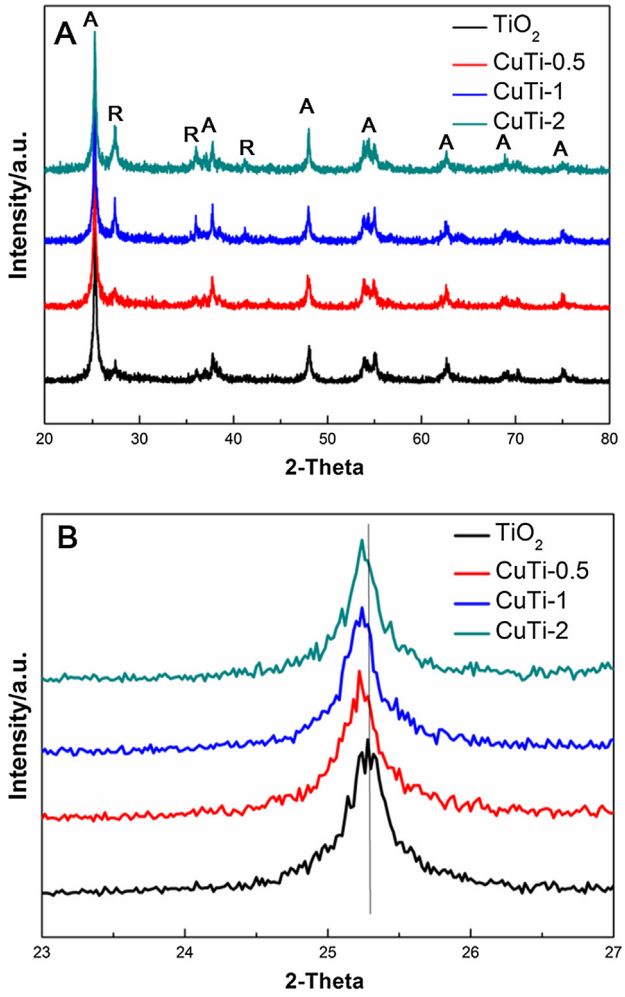

Fig. 1. XRD patterns of CuTi samples (A) and enlarged figure of the main peaks (B).

ca. 932.5 eV and 934.4 eV, respectively. The former is assigned to Cu(I), while the latter is attributed to Cu(II). This indicates that the Cu(II) precursors cannot be completely reduced to Cu(I) during the flame spray pyrolysis process if the concentration of Cu dopant is too high. Combining the results of XRD and TEM, it can be concluded that the Cu^{+} and Cu^{2+} were incorporated into the TiO_2 lattice. Fig. 3B shows that the Ti $2p_{3/2}$ peaks were located at approximately 458.6 eV for all the samples, showing that the Ti in all the samples existed as Ti^{4+} [36,37]. Fig. 3C shows that the O 1s XPS spectra of the CuTi samples can be resolved into two peaks at 529.9 and 531.6 eV, which were attributed to the lattice oxygen in TiO_2 (O_L) and hydroxyl species (O_H), respectively [17].

Table 1 shows that appropriate Cu doping increased the specific surface area of TiO_2, which may be due to the inhibition of the agglomeration of TiO_2 particles by Cu doping, as evident in the TEM images in Fig. 2. However, an excess doping concentration of Cu (> 1%) decreased the specific surface area. This phenomenon was also observed in our previous work, which can be attributed to the increased crystallite size of TiO_2 in the presence of a high doping amount of Cu [30].

Fig. 4 shows the UV–vis DRS of the CuTi catalysts. Compared to TiO_2, the absorption edge of CuTi samples presented a slight redshift, which indicated that the Cu doping enhanced the visible light absorption of TiO_2. Table 1 summarizes the band gaps of CuTi photocatalysts, which decreased with the increase of the Cu concentration. This may be because Cu doping promoted the phase transformation of TiO_2 from anatase to rutile (as shown in Fig. 1 and Table 1), and the latter has a smaller band gap.

The PL spectra in Fig. 5 show that all the samples have two peaks located at approximately 430 and 520 nm, which can be attributed to the band edge free excitons and bound excitons, respectively [13]. For pristine TiO_2, the intensity of the PL peak at 520 nm is weaker than that at 430 nm; however, for CuTi samples, the intensity of the PL peak at 520 nm is stronger. This indicated that more photoinduced electrons were captured on CuTi samples. In addition, the PL intensity remarkably decreased with the increase of the Cu content from 0 to 1%, which demonstrated that Cu^{+} dopants can work as photogenerated electron acceptors and promote the separation of photoexcited charges [9,10]. A similar phenomena was reported by Park et al. [38]. However, the PL intensity increased when the Cu content increased to 2%. This is because excess Cu ions may act as recombination centres for photogenerated electron and hole pairs. It should be noted that in Table 1, the ratio of rutile in CuTi samples increased from TiO_2 to CuTi-2, while the PL intensity decreased first and then increased, which means that the formation of a heterophase junction did not dominate the separation of photogenerated charges.

3.2. CO_2 photocatalytic reduction

The CO and CH_4 yields of CuTi samples are shown in Fig. 6 and Table 2. The main products were detected to be CO and CH_4, while no H_2 existed, which demonstrated that Cu doping prefers the reduction of CO_2 rather than water. The productions of CO and CH_4 of CuTi catalysts were both higher than those of pristine TiO_2. The yields increased as the Cu doping content (0 to 1%) increased. The highest yields of CO (43.5 μmol g^{-1}) and CH_4 (16.7 μmol g^{-1}) were obtained by the CuTi-1 sample after 4 h of irradiation, which were much higher than those reported in the literature [9,20,35]. The production of CO and CH_4 decreased when the Cu doping CO content increased to 2%. This may be caused by the excess doping of Cu, which can work act recombination centres of photogenerated charges, as evident in the PL analysis.

Table 2 shows the quantum efficiencies of photocatalytic CO_2 reduction on CuTi catalysts [39]. For CuTi-1, the quantum efficiencies for CH_4 and CO were 0.0566% and 0.0872%, respectively. Apparently, the quantum efficiencies of the CuTi catalyst were higher than those of TiO_2, showing a higher photon utilization rate of CuTi catalysts.

The cycle performance of CO_2 photoreduction on CuTi-1 is shown in Fig. 7. After each cycle, the reactor was purged with a mixture of CO_2/water vapour, and the same photocatalytic reaction process was restarted. The results show that compared to the first cycle, the performance of CuTi-1 catalysts in the second and third cycles remained nearly unchanged, demonstrating the good stability of CuTi-1 catalyst. To further elucidate this, the chemical states of Cu in CuTi-1 before and after cycles were analysed (Fig. 8). The results show that the chemical states of Cu species before and after cycles did not change, demonstrating that Cu^{+} ions in CuTi-1 were stable during CO_2 photoreduction. In our previous work [23], we found that the Cu_2O deposited on the surface of TiO_2 would be reduced to Cu^{0} after photocatalytic CO_2 reduction. Similar phenomena were also observed in TiO_2 deposited by Cu(I) species reported in the literature [24,26], implying that Cu^{+} doped in the TiO_2 lattice is more stable than that deposited on the surface of TiO_2. This not only explains the stable photocatalytic performance of the CuTi-1 catalyst well but also implies that FSP is an excellent route to prepare stable Cu ion-doped TiO_2 catalyst.

3.3. In situ DRIFTS for CO_2 photoreduction

Fig. 9A shows the in situ DRIFTS of CO_2 and H_2O co-adsorption on CuTi catalysts in the dark. The surface of pristine TiO_2 was dominated by strongly adsorbed water at 1655 cm^{-1}, bidentate carbonate (b-CO_3^{2-}) at 1599 and 1339 cm^{-1} [40], and monodentate carbonate (m-CO_3^{2-}) at 1301 cm^{-1} [41]. For CuTi samples, more new peaks

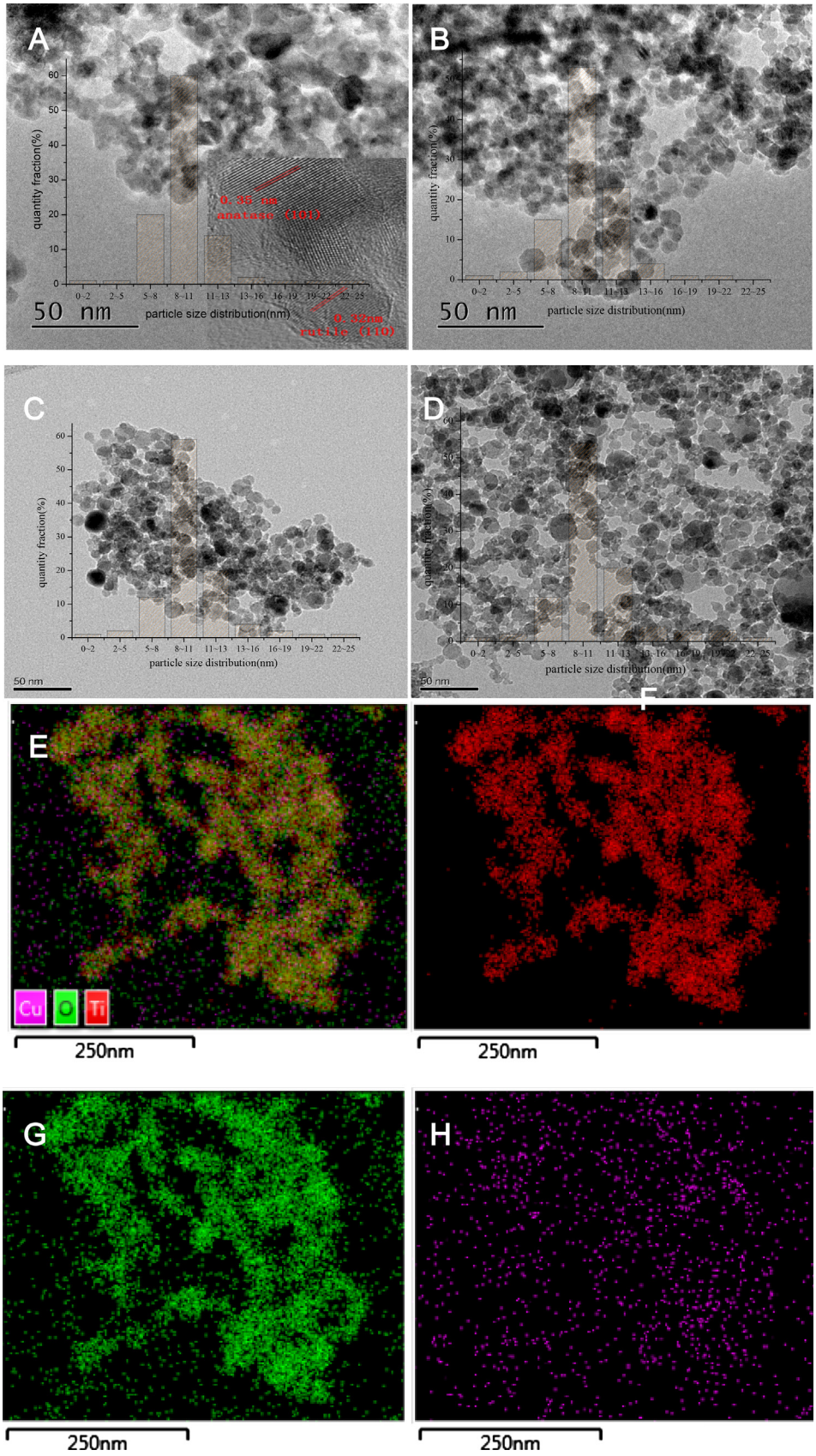

Fig. 2. TEM and HR-TEM images of TiO_2 (A), CuTi-0.5 (B), CuTi-1 (C), and CuTi-2 (D). EELS mapping of Ti (F), O (G), and Cu (H) in CuTi-1.

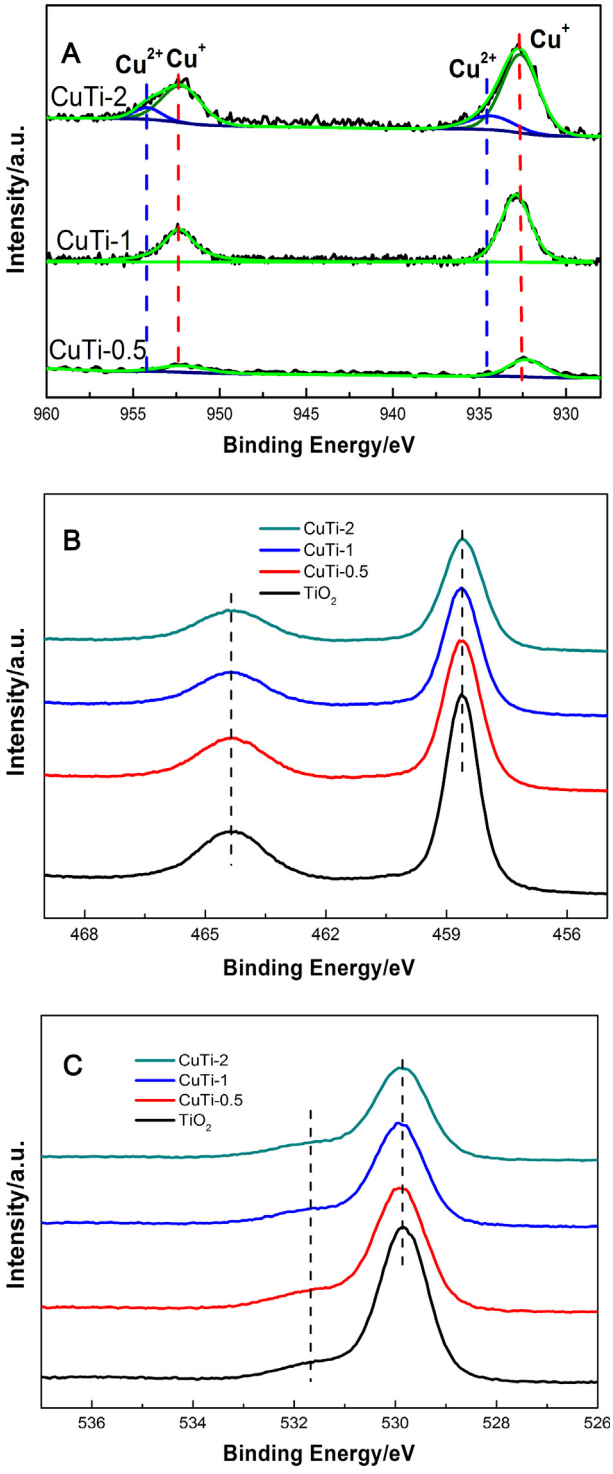

Fig. 3. Cu 2p (A), Ti 2p (B), and O 1s (C) XPS spectra of CuTi catalysts.

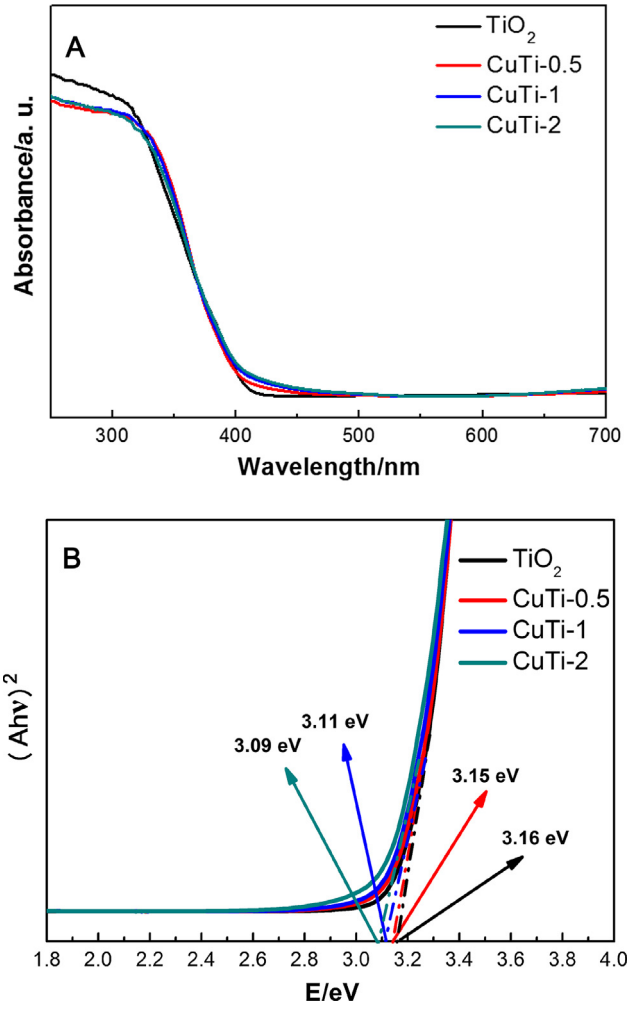

Fig. 4. UV–vis spectra (A) and energy band gap (B) of the catalysts.

appeared at 1682 cm^{-1} (CO_2^-), 1508 cm^{-1} (m-CO_3^{2-}), 1422 cm^{-1} (HCO_3^-), and 1391 cm^{-1} (m-CO_3^{2-}) [42]. In addition, the peak at 1339 cm^{-1} (b-CO_3^{2-}) [40] on CuTi samples becomes stronger after 15 min of adsorption in the dark. The formation of CO_2^- is a very important step of CO_2 photoreduction [40,42]. CO_2^- is generally regarded as a key intermediate of CO_2 reduction, which can finally transform into the target products, such as CO, CH_4, etc. A similar phenomenon can also be observed in Fig. 9B after 15 min of UV light irradiation. These results indicated that the adsorption and activation of CO_2 were promoted by Cu dopant.

In situ DRIFTS for pristine TiO_2 and CuTi-1 during photocatalytic reduction were also recorded to understand the possible transformation of CO_2 species on the surface of the catalyst during the CO_2 photoreduction process. In Fig. 10A, the DRIFTS of pristine TiO_2 under irradiation were almost the same as those in the dark. No CO_2^- or new species were observed, indicating that CO_2 was difficult to activate by pristine TiO_2 under irradiation. However, in Fig. 10B, different results were obtained on CuTi-1. It is notable that, under irradiation, the

Table 1
Summary of physico-chemical properties of the as-prepared samples.

Samples	Anatase/rutile ratio	Bandgap/eV	Pore size/nm	Pore volume/$cm^3\ g^{-1}$	Surface area/$m^2\ g^{-1}$	$Cu^+/Cu^+ + Cu^{2+}$
TiO_2	9:1	3.16	18.37	0.22	47.24	–
CuTi-0.5	8.8:1.2	3.15	28.93	0.79	105.62	100%
CuTi-1	8.2:1.8	3.11	23.48	0.56	99.03	100%
CuTi-2	8.1:1.9	3.09	15.05	0.38	93.58	80%

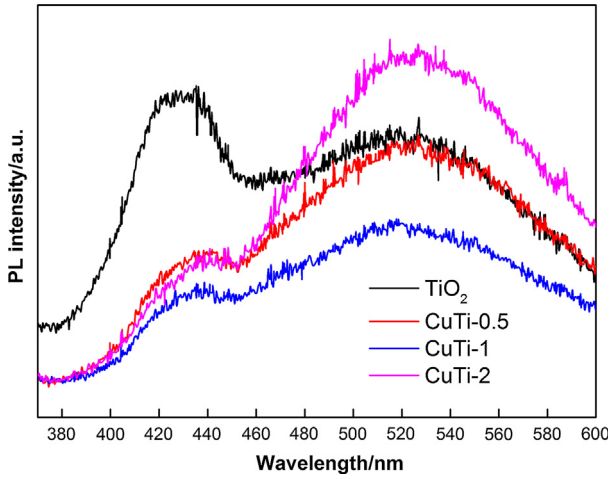

Fig. 5. PL spectra of the as-prepared samples.

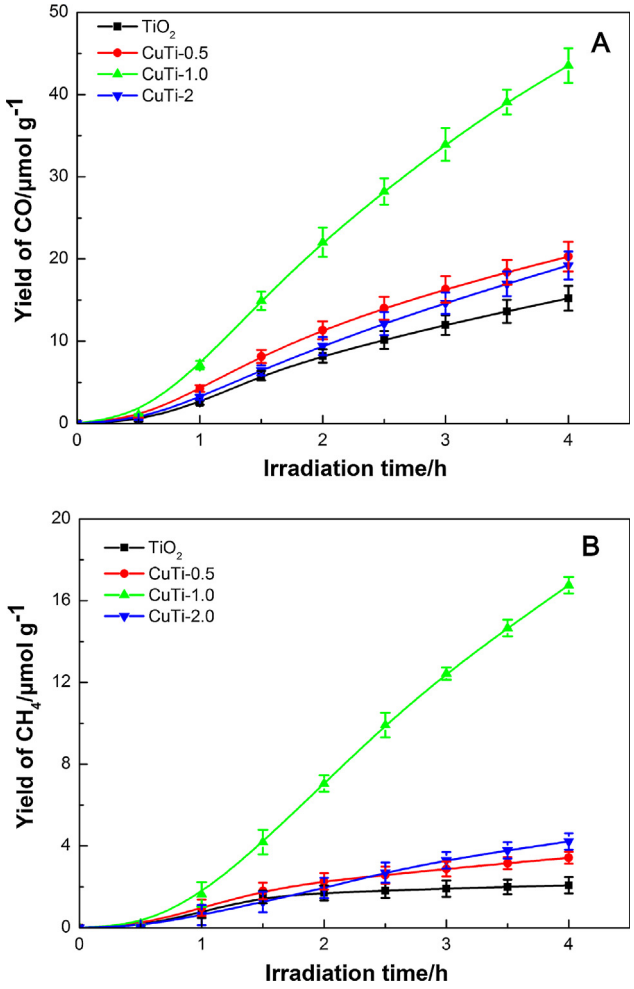

Fig. 6. CO (A) and CH_4 (B) yields over the CuTi catalysts during 4 h light irradiation.

intensity of the IR spectral feature for CO_2^- (1681 cm^{-1}) was enhanced [42], while that of b-CO_3^{2-} (1594 cm^{-1}) decreased [40], which indicates that b-CO_3^{2-} adsorbed on CuTi-1 can be activated by Cu^+ dopant and transform into CO_2^- under UV light irradiation. Therefore, the Cu^+ doped in the TiO_2 lattice enhanced and promoted the adsorption and activation of CO_2 during CO_2 photoreduction.

Combining characterization and in situ DRIFT analysis, it can be concluded that the enhanced and stable activity of CuTi catalysts were ascribed to the highly dispersed and stable Cu^+ ions in the TiO_2 lattice, which increased the surface area, facilitated the separation of photo-excited charges, and promoted the adsorption and activation of CO_2.

Table 2
Photocatalytic activity and quantum efficiency of CuTi catalysts.

Samples	CO/μmol g^{-1} h^{-1}	CH_4/μmol g^{-1} h^{-1}	ΦCO/%	ΦCH_4/%
TiO_2	3.8	0.5	0.0197	0.0104
CuTi-0.5	4.8	0.8	0.0249	0.0166
CuTi-1	10.9	4.2	0.0566	0.0872
CuTi-2	5.1	1.0	0.0265	0.0208

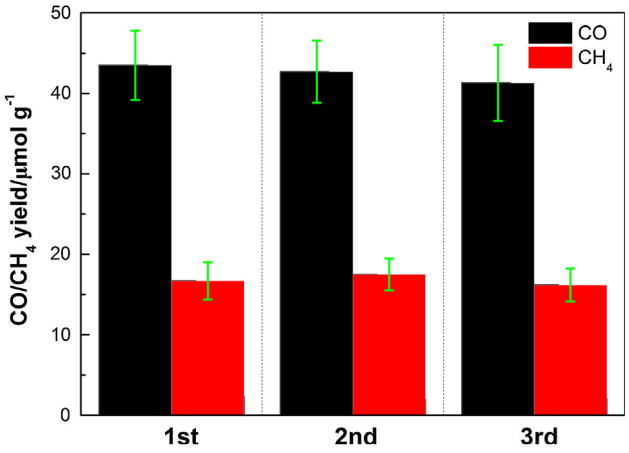

Fig. 7. Cycle performance of CuTi-1 catalyst after 4 h light irradiation.

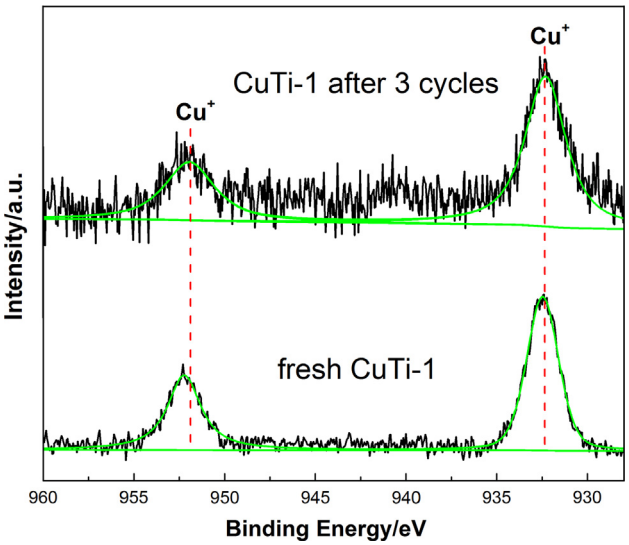

Fig. 8. Cu XPS spectra of CuTi-1 catalyst before reaction and after 3 cycles.

4. Conclusions

Highly dispersed Cu^+-doped TiO_2 catalysts were synthesized though a FSP route. A relatively low Cu doping concentration was found to inhibit the formation of Cu^{2+}. The CuTi catalysts show much higher photocatalytic activity than that of pristine TiO_2. The highest CO and CH_4 yields were obtained on CuTi-1, reaching 43.5 and 16.7 μmol g^{-1}, respectively, after 4 h of irradiation. Cu^+ ions in the TiO_2 lattice inhibited the recombination of photogenerated charges and enhanced the absorption of visible light. The results of DRIFTS show that doped Cu^+ ions enhanced the adsorption and facilitated the

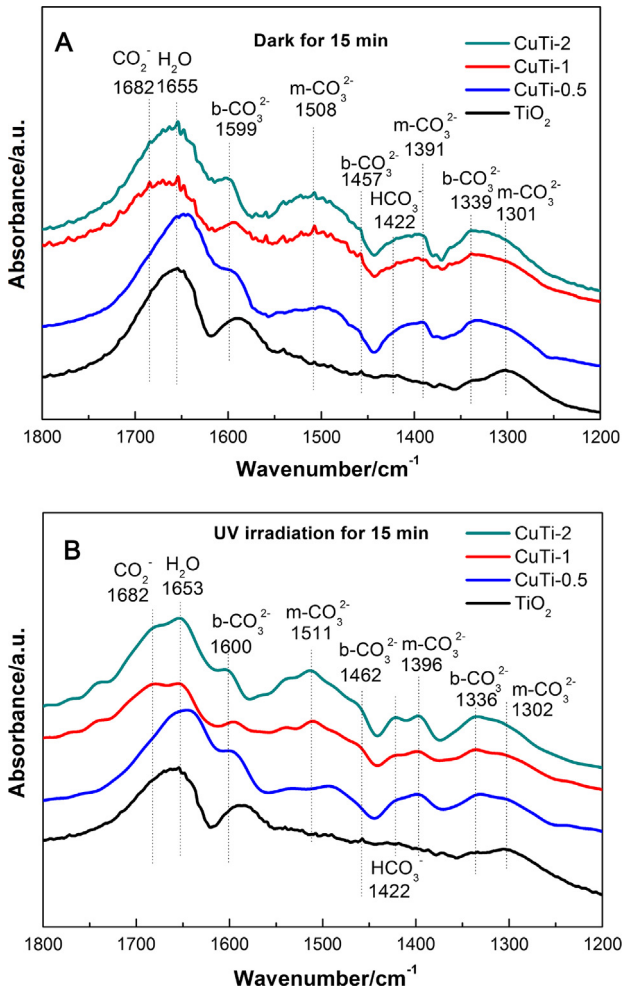

Fig. 9. In situ DRIFTS spectra of CO_2 and H_2O with CuTi catalysts after adsorption in the dark for 15 min (A) and irradiation by UV light for 15 min (B).

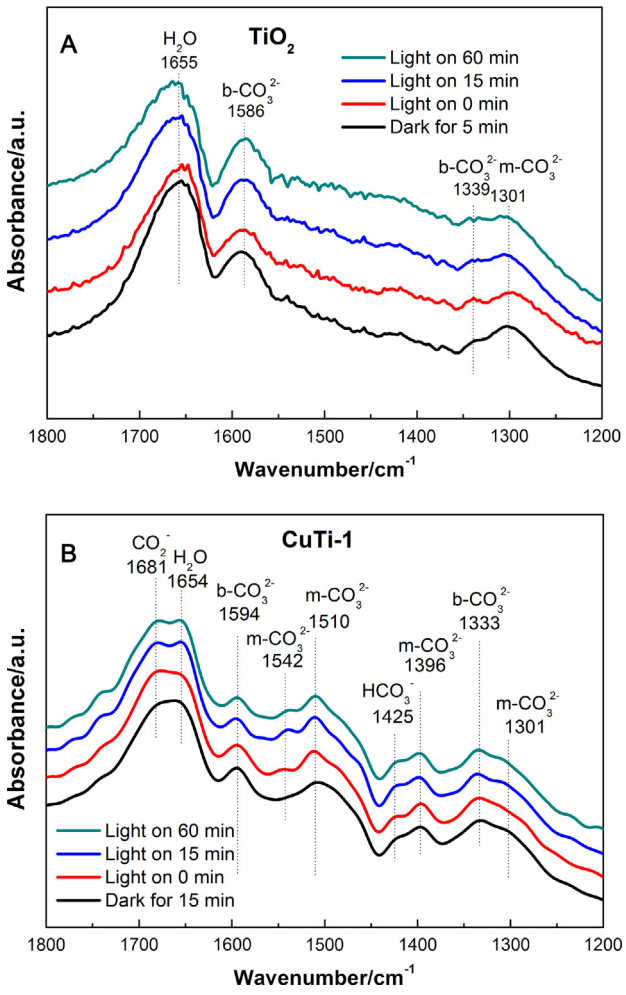

Fig. 10. In situ DRIFTS of CO_2 and H_2O with TiO_2 (A) and CuTi-1 (B) catalysts in the dark, and subsequently irradiated by UV light as a function of time.

activation of CO_2, working as the active sites for CO_2 photoreduction. Furthermore, the Cu^+ ions incorporated into the TiO_2 lattice were very stable during the whole reaction procedure, which explained the good cycle performance of CuTi catalysts. This work not only provides a clearer understanding of the roles of Cu^+ dopant in photocatalytic CO_2 reduction but also provides a novel route to develop efficient and stable ion-doped photocatalysts.

CRediT authorship contribution statement

Zhuo Xiong: Investigation, Writing - original draft, Writing - review & editing, Data curation, Formal analysis. **Zuwei Xu:** Writing - original draft, Investigation, Validation, Data curation. **Youzi Li:** Methodology, Data curation. **Liangchen Dong:** Methodology, Data curation. **Junyi Wang:** Resources, Visualization. **Jiangting Zhao:** Resources, Visualization. **Xiaoxiang Chen:** Investigation, Methodology. **Yongchun Zhao:** Conceptualization, Funding acquisition, Project administration, Writing - review & editing, Supervision. **Haibo Zhao:** Supervision, Conceptualization, Validation, Project administration. **Junying Zhang:** Conceptualization, Methodology, Supervision.

Declaration of Competing Interest

The authors declare that they have no known competing financial interests or personal relationships that could have appeared to influence the work reported in this paper.

Acknowledgments

This project was supported by the National Natural Science Foundation of China (U1610110, 51706082, and 51606079), the Fundamental Research Funds for the Central Universities, HUST (2019kfyXJJS111). The authors acknowledge the Analysis and Test Center of Huazhong University of Science & Technology.

References

[1] Y.-H. Cheng, V.-H. Nguyen, H.-Y. Chan, J.C.S. Wu, W.-H. Wang, Photo-enhanced hydrogenation of CO_2 to mimic photosynthesis by CO co-feed in a novel twin reactor, Appl. Energy 147 (2015) 318–324.
[2] W. Li, Y. Shi, Y. Luo, Y. Wang, N. Cai, Carbon monoxide/carbon dioxide electrochemical conversion on patterned nickel electrodes operating in fuel cell and electrolysis cell modes, Int. J. Hydrogen Energy 41 (2016) 3762–3773.
[3] W.-H. Lee, C.-H. Liao, M.-F. Tsai, C.-W. Huang, J.C.S. Wu, A novel twin reactor for CO_2 photoreduction to mimic artificial photosynthesis, Appl. Catal. B 132–133 (2013) 445–451.
[4] Z. Xiong, Z. Lei, Y. Li, L. Dong, Y. Zhao, J. Zhang, A review on modification of facet-engineered TiO_2 for photocatalytic CO_2 reduction, J. Photochem. Photobiol., C 36 (2018) 24–47.
[5] T. Inoue, A. Fujishima, S. Konishi, K. Honda, Photoelectrocatalytic reduction of carbon dioxide in aqueous suspensions of semiconductor powders, Nature 277 (1979) 637–638.
[6] Z. Xiong, Y. Zhao, J. Zhang, C. Zheng, Efficient photocatalytic reduction of CO2 into liquid products over cerium doped titania nanoparticles synthesized by a sol–gel auto-ignited method, Fuel Process. Technol. 135 (2015) 6–13.
[7] C.-W. Huang, C.-H. Liao, J.C.S. Wu, Y.-C. Liu, C.-L. Chang, C.-H. Wu, M. Anpo, M. Matsuoka, M. Takeuchi, Hydrogen generation from photocatalytic water splitting over TiO_2 thin film prepared by electron beam-induced deposition, Int. J. Hydrogen Energy 35 (2010) 12005–12010.

[8] M. Pelaez, N.T. Nolan, S.C. Pillai, M.K. Seery, P. Falaras, A.G. Kontos, P.S.M. Dunlop, J.W.J. Hamilton, J.A. Byrne, K. O'Shea, M.H. Entezari, D.D. Dionysiou, A review on the visible light active titanium dioxide photocatalysts for environmental applications, Appl. Catal. B 125 (2012) 331–349.

[9] Q. Zhang, T. Gao, J.M. Andino, Y. Li, Copper and iodine co-modified TiO_2 nanoparticles for improved activity of CO_2 photoreduction with water vapor, Appl. Catal. B 123–124 (2012) 257–264.

[10] M. Tahir, N.S. Amin, Photocatalytic CO_2 reduction with H_2 as reductant over copper and indium co-doped TiO_2 nanocatalysts in a monolith photoreactor, Appl. Catal. A 493 (2015) 90–102.

[11] Y. Li, W. Zhang, X. Shen, P. Peng, L. Xiong, Y. Yu, Octahedral Cu_2O-modified TiO_2 nanotube arrays for efficient photocatalytic reduction of CO_2, Chin. J. Catal. 36 (2015) 2229–2236.

[12] W.N. Wang, W.J. An, B. Ramalingam, S. Mukherjee, D.M. Niedzwiedzki, S. Gangopadhyay, P. Biswas, Size and structure matter: Enhanced CO_2 photoreduction efficiency by size-resolved ultrafine Pt nanoparticles on TiO_2 single crystals, J. Am. Chem. Soc. 134 (2012) 11276–11281.

[13] Z. Xiong, H. Wang, N. Xu, H. Li, B. Fang, Y. Zhao, J. Zhang, C. Zheng, Photocatalytic reduction of CO_2 on Pt^{2+}–Pt^0/TiO_2 nanoparticles under UV/Vis light irradiation: a combination of Pt^{2+} doping and Pt nanoparticles deposition, Int. J. Hydrogen Energy 40 (2015) 10049–10062.

[14] Z. Xiong, Z. Lei, X. Chen, B. Gong, Y. Zhao, J. Zhang, C. Zheng, J.C.S. Wu, CO2 photocatalytic reduction over Pt deposited TiO2 nanocrystals with coexposed 101 and 001 facets: effect of deposition method and Pt precursors, Catal. Commun. 96 (2017) 1–5.

[15] C. Zhao, A. Krall, H. Zhao, Q. Zhang, Y. Li, Ultrasonic spray pyrolysis synthesis of Ag/TiO_2 nanocomposite photocatalysts for simultaneous H_2 production and CO_2 reduction, Int. J. Hydrogen Energy 37 (2012) 9967–9976.

[16] H. Li, X. Wu, J. Wang, Y. Gao, L. Li, K. Shih, Enhanced activity of Ag-MgO-TiO_2 catalyst for photocatalytic conversion of CO_2 and H_2O into CH_4, Int. J. Hydrogen Energy 41 (2016) 8479–8488.

[17] D. Kong, J.Z.Y. Tan, F. Yang, J. Zeng, X. Zhang, Electrodeposited Ag nanoparticles on TiO_2 nanorods for enhanced UV visible light photoreduction CO_2 to CH_4, Appl. Surf. Sci. 277 (2013) 105–110.

[18] I.H. Tseng, J.C.S. Wu, H.-Y. Chou, Effects of sol–gel procedures on the photocatalysis of Cu/TiO_2 in CO_2 photoreduction, J. Catal. 221 (2004) 432–440.

[19] D. Liu, Y. Fernández, O. Ola, S. Mackintosh, M. Maroto-Valer, C.M.A. Parlett, A.F. Lee, J.C.S. Wu, On the impact of Cu dispersion on CO_2 photoreduction over Cu/TiO_2, Catal. Commun. 25 (2012) 78–82.

[20] L. Liu, F. Gao, H. Zhao, Y. Li, Tailoring Cu valence and oxygen vacancy in Cu/TiO_2 catalysts for enhanced CO_2 photoreduction efficiency, Appl. Catal. B 134–135 (2013) 349–358.

[21] H. Tian, K. Cheng, Y. Wang, D. Zhao, F. Chai, Z. Xue, J. Hao, Quantitative assessment of variability and uncertainty of hazardous trace element (Cd, Cr, and Pb) contents in chinese coals by using bootstrap simulation, J. Air Waste Manag. Assoc. 61 (2011) 755–763.

[22] B.R. Chen, V.H. Nguyen, J.C. Wu, R. Martin, K. Koci, Production of renewable fuels by the photohydrogenation of CO_2: effect of the Cu species loaded onto TiO_2 photocatalysts, PCCP 18 (2016) 4942–4951.

[23] Z. Xiong, Z. Lei, C.-C. Kuang, X. Chen, B. Gong, Y. Zhao, J. Zhang, C. Zheng, J.C.S. Wu, Selective photocatalytic reduction of CO_2 into CH_4 over Pt-Cu_2O TiO_2 nanocrystals: the interaction between Pt and Cu_2O cocatalysts, Appl. Catal. B 202 (2017) 695–703.

[24] Y. Li, W.-N. Wang, Z. Zhan, M.-H. Woo, C.-Y. Wu, P. Biswas, Photocatalytic reduction of CO_2 with H_2O on mesoporous silica supported Cu/TiO_2 catalysts, Appl. Catal. B 100 (2010) 386–392.

[25] J.Z.Y. Tan, Y. Fernández, D. Liu, M. Maroto-Valer, J. Bian, X. Zhang, Photoreduction of CO_2 using copper-decorated TiO_2 nanorod films with localized surface plasmon behavior, Chem. Phys. Lett. 531 (2012) 149–154.

[26] L. Yuan, S.-F. Hung, Z.-R. Tang, H.M. Chen, Y. Xiong, Y.-J. Xu, Dynamic evolution of atomically dispersed Cu species for CO_2 photoreduction to solar fuels, ACS Catal. (2019) 4824–4833.

[27] X. Chen, Z. Xu, F. Yang, H. Zhao, Flame spray pyrolysis synthesized CuO-TiO_2 nanoparticles for catalytic combustion of lean CO, Proc. Combust. Inst. 37 (2019) 5499–5506.

[28] F. Yang, M. Liu, X. Chen, Z. Xu, H. Zhao, Simultaneous control over lattice doping and nanocluster modification of a hybrid CuO_x/TiO_2 photocatalyst during flame synthesis for enhancing hydrogen evolution, Solar RRL 2 (2018) 1800215.

[29] Z. Xiong, Z. Lei, Z. Xu, X. Chen, B. Gong, Y. Zhao, H. Zhao, J. Zhang, C. Zheng, Flame spray pyrolysis synthesized ZnO/CeO2 nanocomposites for enhanced CO2 photocatalytic reduction under UV–Vis light irradiation, J. CO2 Util. 18 (2017) 53–61.

[30] X. Chen, Z. Xu, F. Yang, H. Zhao, Flame spray pyrolysis synthesized CuO-TiO_2 nanoparticles for catalytic combustion of lean CO, Proc. Combust. Inst. 000 (2018) 1–8.

[31] Z. Xiong, Y. Luo, Y. Zhao, J. Zhang, C. Zheng, J.C. Wu, Synthesis, characterization and enhanced photocatalytic CO2 reduction activity of graphene supported TiO2 nanocrystals with coexposed 001 and 101 facets, PCCP 18 (2016) 13186–13195.

[32] R. Kydd, W.Y. Teoh, K. Wong, Y. Wang, J. Scott, Q.-H. Zeng, A.-B. Yu, J. Zou, R. Amal, Flame-synthesized ceria-supported copper dimers for preferential oxidation of CO, Adv. Funct. Mater. 19 (2009) 369–377.

[33] M.S.P. Francisco, V.R. Mastelaro, Inhibition of the anatase-rutile phase transformation with addition of CeO_2 to CuO-TiO_2 system raman spectroscopy, X-ray diffraction, and textural studies, Chem. Mater. 14 (2002) 2514–2518.

[34] L. Matějová, K. Kočí, M. Reli, L. Čapek, A. Hospodková, P. Peikertová, Z. Matěj, L. Obalová, A. Wach, P. Kuśtrowski, A. Kotarba, Preparation, characterization and photocatalytic properties of cerium doped TiO_2: on the effect of Ce loading on the photocatalytic reduction of carbon dioxide, Appl. Catal. B 152–153 (2014) 172–183.

[35] Q. Zhai, S. Xie, W. Fan, Q. Zhang, Y. Wang, W. Deng, Y. Wang, Photocatalytic conversion of carbon dioxide with water into methane: platinum and copper(I) oxide co-catalysts with a core-shell structure, Angew. Chem. 52 (2013) 5776–5779.

[36] L. Zhang, R.V. Koka, A study on the oxidation and carbon diffusion of TiC in alumina–titanium carbide ceramics using XPS and Raman spectroscopy, Mater. Chem. Phys. 57 (1998) 23–32.

[37] B. Fang, N.K. Chaudhari, M.-S. Kim, J.H. Kim, J.-S. Yu, Homogeneous deposition of platinum nanoparticles on carbon black for proton exchange membrane fuel cell, J. Am. Chem. Soc. 131 (2009) 15330–15338.

[38] S.-M. Park, A. Razzaq, Y.H. Park, S. Sorcar, Y. Park, C.A. Grimes, S.-I. In, Hybrid Cu x O-TiO2 Heterostructured composites for photocatalytic CO2 reduction into methane using solar irradiation: sunlight into fuel, ACS Omega 1 (2016) 868–875.

[39] B. Fang, A. Bonakdarpour, K. Reilly, Y. Xing, F. Taghipour, D.P. Wilkinson, Large-scale synthesis of TiO_2 microspheres with hierarchical nanostructure for highly efficient photodriven reduction of CO_2 to CH_4, ACS Appl. Mater. Interfaces 6 (2014) 15488–15498.

[40] Y. Wang, J. Zhao, T. Wang, Y. Li, X. Li, J. Yin, C. Wang, CO_2 photoreduction with H_2O vapor on highly dispersed CeO_2/TiO_2 catalysts: Surface species and their reactivity, J. Catal. 337 (2016) 293–302.

[41] L. Liu, H. Zhao, J.M. Andino, Y. Li, Photocatalytic CO_2 reduction with H_2O on TiO_2 nanocrystals: Comparison of anatase, rutile, and brookite polymorphs and exploration of surface chemistry, ACS Catal. 2 (2012) 1817–1828.

[42] L. Liu, Y. Jiang, H. Zhao, J. Chen, J. Cheng, K. Yang, Y. Li, Engineering coexposed 001 and 101 facets in oxygen-deficient TiO2 nanocrystals for enhanced CO2 photoreduction under visible light, ACS Catal. 6 (2016) 1097–1108.